WILEY ONLINE LIBRARY
Early View publication on
www.wileyonlinelibrary.com
(issue and page numbers not yet assigned;
citable using Digital Object Identifier – **DOI**)

J. Biophotonics 1–8 (2013) / **DOI** 10.1002/jbio.201300012

Journal of
BIOPHOTONICS

FULL ARTICLE

A silicon photonic biosensor using phase-shifted Bragg gratings in slot waveguide

Xu Wang[*,1], *Jonas Flueckiger*[1], *Shon Schmidt*[2], *Samantha Grist*[1], *Sahba T. Fard*[1], *James Kirk*[2], *Matt Doerfler*[2], *Karen C. Cheung*[1], *Daniel M. Ratner*[2], *and Lukas Chrostowski*[1]

[1] Department of Electrical and Computer Engineering, University of British Columbia, Vancouver, BC V6T 1Z4, Canada
[2] Department of Bioengineering, University of Washington, Seattle, WA 98195, USA

Received 19 January 2013, revised 12 March 2013, accepted 13 March 2013
Published online 15 April 2013

Key words: biosensor, silicon photonics, slot waveguide, Bragg grating, microfluidics, limit of detection

We present a novel silicon photonic biosensor using phase-shifted Bragg gratings in a slot waveguide. The optical field is concentrated inside the slot region, leading to efficient light-matter interaction. The Bragg gratings are formed with sidewall corrugations on the outside of the waveguide, and a phase shift is introduced to create a sharp resonant peak within the stop band. We experimentally demonstrate a high sensitivity of 340 nm/RIU measured in salt solutions and a high quality factor of 1.5×10^4, enabling a low intrinsic limit of detection of 3×10^{-4} RIU. Furthermore, the silicon device was fabricated by a CMOS foundry, facilitating high-volume and low-cost production. Finally, we demonstrate the device's ability to interrogate specific biomolecular interactions, resulting in the first of its kind label-free biosensor.

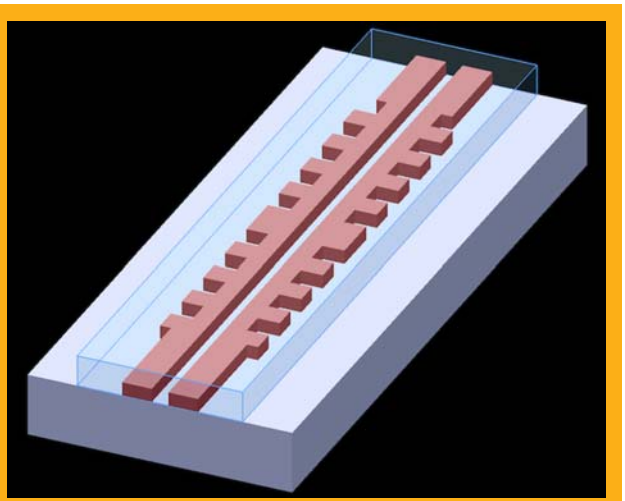

Schematic diagram of the sensor.

1. Introduction

Silicon photonic biosensors have demonstrated great potential for label-free on-chip detection of biomolecules [1, 2]. Various optical structures [3, 4], such as microring [5–11] and microdisk resonators [1], Bragg gratings [12], and photonic crystals [13–15], have been developed on the silicon-on-insulator (SOI) platform for biological sensing applications. Nearly all of these sensors are based on measuring the change in the refractive index (RI) of the surrounding environment, which allows for real-time and direct detection of molecular interactions near the sensor surface. Fundamentally, the sensitivity is determined by the overlap between the electric field and the analyte. In many silicon photonic sensors (e.g., strip-waveguide-based ring resonators [5–11] and Bragg gratings [12], disk resonators [1], conven-

* Corresponding author: e-mail: xuw@ece.ubc.ca

tional photonic crystals [13, 14]), the majority of the electric field is confined in the high-index material (i.e., silicon), thus it is difficult to interact with the analyte efficiently and the sensitivity is low. To enhance the sensitivity, an effective solution is to use slot waveguide structures [16, 17]. In slot waveguides, the electric field is concentrated inside the low-index slot, leading to an increased field overlap with the analyte and hence a higher sensitivity. A slot waveguide ring resonator was first developed for biosensing applications by Barrios et al. [18] on a Si_3N_4–SiO_2 platform, showing a bulk sensitivity of 212 nm/RIU (refractive index unit). This structure has also been demonstrated on the SOI platform by Claes et al. [19], showing a higher sensitivity of 298 nm/RIU, as well as a much smaller footprint due to the high index contrast of the material system.

The limit of detection (LOD) is another important parameter to evaluate the sensor performance, which is often defined as the minimum detectable RI change. For single-resonator silicon photonic sensors, the LOD depends not only on the sensitivity but also on the resonance quality (Q) factor and the system noise [1, 20]. For the purpose of comparing different single-resonator sensors (neglecting the measurement system noise), the intrinsic LOD can be defined as the RI change corresponding to one resonance linewidth, which is inversely proportional to the sensitivity and the Q factor [1]. Therefore, it is necessary to have both high sensitivity and high Q factor to minimize the intrinsic LOD. The aforementioned slot waveguide ring resonators have shown high sensitivities, however, their Q factors are typically very low, which is primarily limited by high bending loss, scattering loss from waveguide roughness, and mode mismatch loss [19]. Although Baehr-Jones et al. [21] demonstrated slot ring resonators with exceptionally high Q values (>20,000 in air) in 2005, they pointed out that there are significant challenges in the design and fabrication. Thus, their record Q values have not been reproduced since then, and in fact, other reported Q values since then are much lower (e.g., Barrios et al. reported $Q = 330$ in Ref. [18] and Claes et al. reported $Q = 1800$ in Ref. [19], both in water). Moreover, in general, ring resonators have limited free spectral ranges (FSR) and demanding tolerance on the structural geometry (e.g., in order to achieve a high extinction ratio, the critical coupling condition must be satisfied, which requires a strict control of the coupling region). Recently, another structure called a slotted photonic crystal [22, 23] has gained attention in this field due to its small modal volume and greatly enhanced light-matter interaction. However, it presents additional design and fabrication challenges.

In this paper, we propose a simple optical biosensor using phase-shifted Bragg gratings in a slot waveguide and demonstrate it on the SOI platform. Since the device is based on a slot waveguide, its sensitivity is expected to be comparable to that of slot waveguide ring resonators [18, 19]. A phase-shifted Bragg grating structure [24–26] is built on the slot waveguide and generates a sharp resonance peak in the transmission spectrum. This peak exhibits a significantly enhanced Q factor compared to slot waveguide ring resonators, since it does not suffer from the aforementioned bending and mode mismatch losses. Therefore, by combining the high sensitivity of the slot with the high Q factor of the phase-shifted Bragg gratings, we obtain an intrinsic LOD of 3×10^{-4} RIU at 1550 nm. To our knowledge, this is the best experimental result for slot-based biosensors.

Additional advantages of this sensor include simple optical design, a high extinction ratio, a small footprint, a large range for RI change (owing to single-mode operation), rapid integration with microfluidic channels, and compatibility with commercial CMOS fabrication technology. Commercial CMOS compatibility is particularly important for producing high-volume, low-cost, and possibly disposable sensor chips by leveraging the economies of scale of the CMOS foundry process [27, 28].

To evaluate the performance of this sensor, the silicon chip is integrated with a reversibly bonded polydimethylsiloxane (PDMS) microfluidic chip. We observe that the experimental performance of the sensor is in excellent agreement with numerical simulations. The performance of the biosensor in a modified biological sandwich assay is also presented.

2. Experiments

2.1 Optics

Figure 1 shows the schematic diagram of the sensor. The device is designed on a high-index-contrast SOI platform with a 220 nm silicon layer on top of a 2 μm buried oxide layer. The slot waveguide is formed in the silicon layer, consisting of two silicon arms separated by a low-index slot region. The waveguide cross section, together with the simulated mode profile, is shown in Figure 2. The slot width and the arm width are designed to be 150 nm and 270 nm, respectively, chosen to be compatible with the CMOS foundry design rules. As shown in Figure 2, the quasi-transverse-electric (TE) mode has a high optical intensity inside the slot region. This unique property makes the slot waveguide much more sensitive to the surrounding fluidics than conventional strip waveguides that use only weak evanescent field tails. The slot waveguide also has weak evanescent field decaying on the outer sides of the

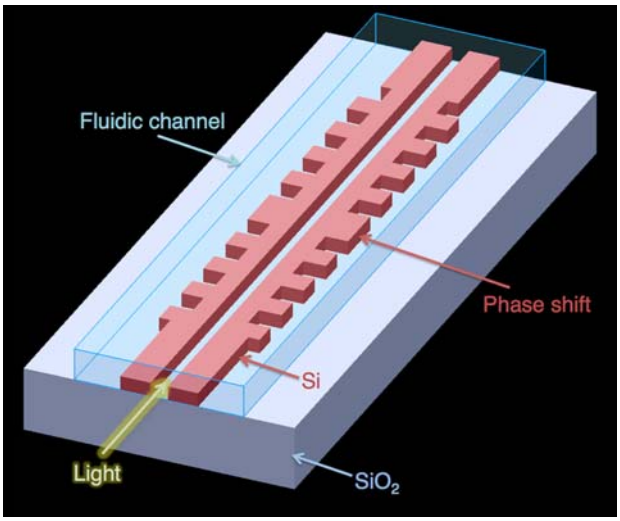

Figure 1 Schematic diagram of the sensor integrated with microfluidic channel.

waveguide, which slightly add to the light-matter interaction, and, as will be discussed below, is used for the construction of Bragg gratings.

As shown in Figure 1, the Bragg gratings are formed by corrugating the outer sidewalls of the slot waveguide, where the weak evanescent field decays. The width of the corrugation on each side is designed to be 40 nm (i.e., the arm width is 270 ± 20 nm). As the light propagates through the waveguide, the effective index of the guided mode is modulated by the corrugations, leading to a stop band in the transmission spectrum. The grating period is designed to be 440 nm, with a duty cycle of 50%, and the simulated Bragg wavelength is around 1530 nm when the cladding is water ($n = 1.33$). To obtain a sharp resonance peak in the stop band, a phase shift is introduced into the middle of the gratings, thus constructing a first-order Fabry–Perot cavity with mirrors formed by two Bragg reflectors [29]. There are 150 pairs of gratings on each side of the phase shift; therefore, the total length of the sensor is about 132 μm. The footprint, however, is still small because the sensor is a waveguide that is less than 1 μm wide, with a total area smaller than 132 μm^2.

The silicon devices were fabricated on a 200 mm SOI wafer using 193 nm deep-ultraviolet (DUV) lithography and dry etching. The fabrication was done at imec through the ePIXfab multi-project wafer service [30]. The fabrication process is compatible with standard CMOS technology and offers high resolution and mass production capabilities. Figure 3 shows a scanning electron microscope (SEM) image of the fabricated device. Note that we used square corrugations in the mask layout, however, the gratings actually fabricated are smoothed due to lithographic effects during fabrication, as clearly shown in Figure 3. Such smoothing effect is common to the fabrication of Bragg gratings on waveguide sidewalls using DUV lithography [31–33], however, it can be predicted using lithography simulations [34].

In our experiments, light is coupled in and out of the silicon chip via integrated fiber-to-waveguide grating couplers [35]. The grating couplers are placed far away from the sensing devices in the microfluidic channels. In order to minimize the waveguide propagation losses, we used a conventional strip waveguide (500 nm wide) as the routing waveguide. A compact strip-to-slot mode converter similar to Ref. [36] was designed for the transition be-

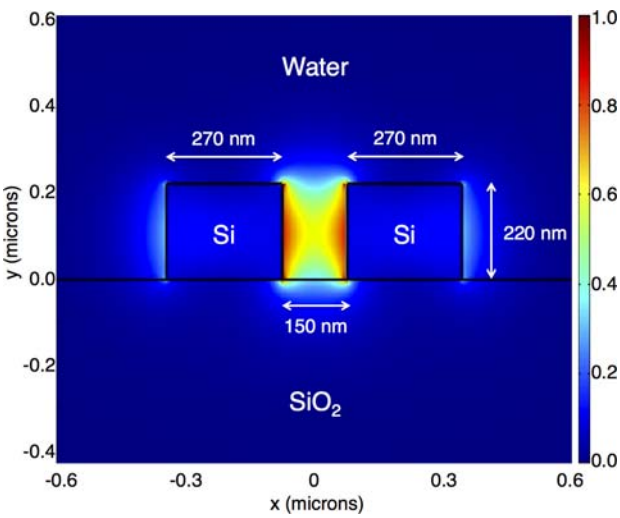

Figure 2 Cross section and mode profile for the slot waveguide immersed in water. The mode profile is calculated using Lumerical MODE Solutions eigensolver.

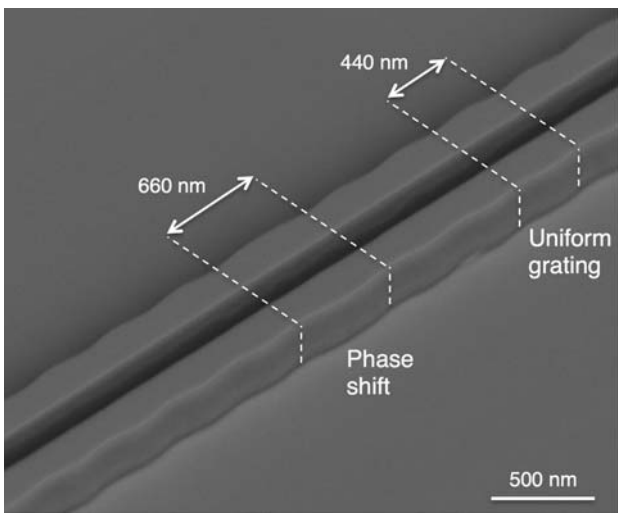

Figure 3 SEM image of a fabricated device. Note that the phase shift in the central region can be identified by measuring the spacing between the grating grooves. Here, the spacing with the phase shift is 660 nm, corresponding to 1.5 times the grating period.

tween the strip and slot waveguides. The optical transmission spectrum was characterized using an automated fiber array test station, which consists of a tunable laser source with a wide tuning range and a small wavelength resolution of 0.5 pm, polarization maintaining fiber arrays, optical power meters, and an automated micro-positioning stage for fiber alignment.

2.2 Microfluidics and sensing experiments

The microfluidic channels were fabricated using polydimethylsiloxane (PDMS) soft lithography [37]. Briefly, SU-8 photoresist (MicroChem) was spin cast onto standard silicon wafers to a thickness of approximately 80 μm. It was patterned using UV exposure through a transparency mask containing the microfluidic channel designs. After resist development PDMS prepolymer and curing agent (Sylgard), mixed at a ratio of 10 : 1, were cast onto the mold and cured. The PDMS was then demolded and the individual microfluidic chips were diced and their inlet and outlet holes bored. Fluidic connections were made using friction fit fluid dispensing tips (EFD) interfaced with standard silastic tubing and connected to a syringe pump (Chemyx Nexus 3000).

NaCl solutions of varying concentrations (in deionized water) were used for the refractive index sensitivity calibration of the sensor. For these experiments, the syringe pump was used to deliver deionized water, 62.5 mM, 125 mM, 250 mM, and 500 mM solutions through the microfluidic channels atop the sensors, interrupting flow briefly between reagent changes. The refractive indices of these solutions were measured using a digital refractometer (Reichert AR200).

3. Results and discussion

3.1 Optical spectrum

Figure 4 shows the measured transmission spectrum of the sensor immersed in deionized water. As expected, a sharp resonance peak appears at the centre of the stop band. The linewidth of this resonance (full width at half-maximum, FWHM) is about 0.1 nm, corresponding to a Q factor of about 1.5×10^4. This "in-water" Q factor is much higher than those of the reported slot waveguide ring resonators [18, 19] and the slotted photonic crystal cavities [22]. Also of interest is that the resonance peak exhibits a large extinction ratio of more than 20 dB, which is rarely seen in other slot-based biosensors

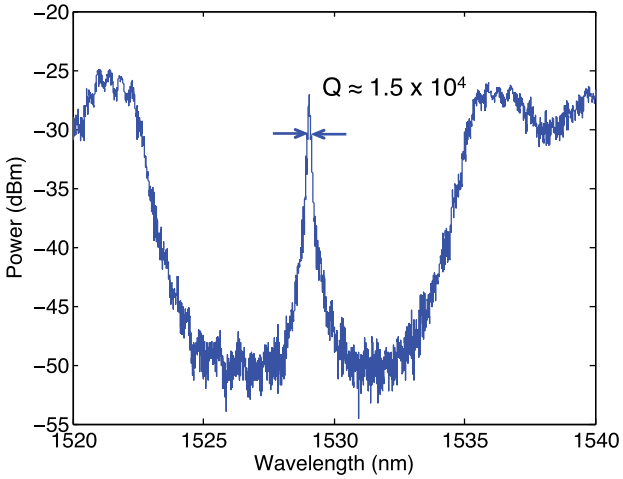

Figure 4 Measured transmission spectrum of the sensor immersed in deionized water.

such as ring resonators. As this work is a proof-of-concept, we expect that the Q factor can be further improved. For a phase-shifted Bragg grating, the Q factor depends on the coupling and the waveguide loss [24]. The coupling is determined by the grating strength and length, both of which are adjustable. The waveguide loss, by contrast, is intrinsic as it arises from the waveguide roughness and water absorption. Therefore, the Q factor will be ultimately limited by the waveguide loss. To optimize the Q factor, the general approach is to increase the strength and/or length of the gratings until it reaches critical coupling condition [1] so that both high Q and high peak amplitude are attainable. Shifting to the 1300 nm window should also improve the Q factor because the water absorption is much lower than at 1550 nm.

3.2 RI sensitivity

Figure 5(a) shows the measured transmission spectra of the sensor covered with different NaCl concentrations. For each concentration, we measured the optical spectra multiple times (every ∼1.5 minutes) to verify the reliability and repeatability. The peak wavelength shift during the six steps is also shown in Figure 5(b). Since the refractive indices of the salt solutions are already known, we plot the peak wavelength shift as a function of the refractive index in Figure 6. We clearly observe that the experimental result agrees well with the simulation result. The sensitivity (S) is 340 nm/RIU, which is higher than those of the reported slot waveguide ring resonators [18, 19, 38–40]. We think that the sensitivity can be further improved by optimizing the waveguide cross section [17] (e.g. by decreasing the arm width).

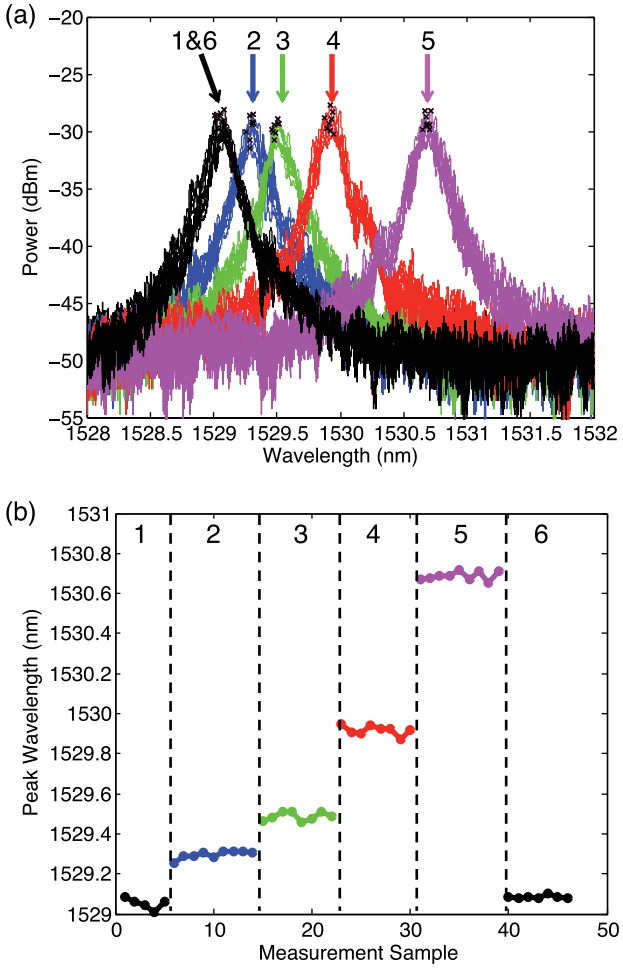

Figure 5 Measurement results for different NaCl concentrations: (**a**) transmission spectra for all the measurements, (**b**) peak wavelength shift during the salt steps. Each color represents a NaCl concentration. Step 1 and 6 correspond to 0 mM, and Step 2 to 5 correspond to 62.5 mM, 125 mM, 250 mM, and 500 mM solutions, respectively.

Based on the Q factor and the sensitivity, we can obtain the intrinsic LOD [1]:

$$\mathrm{LOD}_{\mathrm{intrinsic}} = \Delta n_{\mathrm{min}} = \frac{\lambda}{QS} = 3 \times 10^{-4} \quad (1)$$

This intrinsic LOD is, to date, the best experimental result for slot-based biosensors. Additionally, the theoretical limit for the intrinsic LOD for an ideal water-based single-resonator sensor operating at 1550 nm is 2.4×10^{-4} RIU [1], hence this slot-based sensor performs close to the theoretical limit.

3.3 Biosensing

To demonstrate the biosensing capability, we conducted a modified sandwich assay involving well-characterized biomolecules with high binding affinities. The results, together with the accompanying reagent sequencing, are shown in Figure 7(a) and (b) respectively. Reagents were delivered to the sensor at 10 µL/min via reversibly-bonding PDMS microfluidics, briefly pausing flow to switch reagents. To limit the effects of thermal drift, the optical stage was thermally controlled to 30 °C, thereby negating minor perturbations in the ambient temperature of the room. Optical scans of the resonant peaks were taken every 45 seconds and a signal baseline was established using phosphate buffered saline (PBS) for 20 minutes prior to sequencing other reagents. Lorentzian fitting of the optical spectra was used to determine the resonance wavelength.

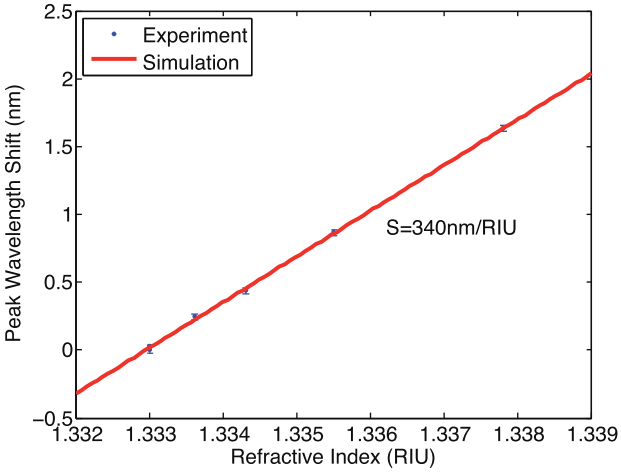

Figure 6 Measured and simulated peak wavelength shift as a function of the refractive index of the salt solution. For the experimental data, the symmetric error bars are two standard deviation units in length.

To orient the capture antibody on the sensor surface, Protein-A (1 mg/mL) was passively adsorbed to its surface [41, 42] followed by a PBS wash to remove unbound or loosely bound protein as shown in region [A] of Figure 7(a) and (b). Next, the capture antibody, anti-Streptavidin (antiSA, 125 µg/mL), was introduced to functionalize the sensor's surface. Upon adsorption, the 160 kDa protein results in a 2 nm resonant wavelength shift, as can be clearly seen in region [B]. To ensure our biological interactions were specific, the functionalized sensor was challenged with bovine serum albumin (BSA, 2 mg/mL), as shown in Region [C]. After a PBS wash, the signal drops towards the pre-BSA baseline, as expected. We hypothesize that the slight residual BSA is the result of incomplete rinsing by PBS or by permanent adsorption of BSA to the sensor surface resulting from incomplete coverage of the first Protein-A monolayer [43]. Next, we introduced the target analyte, Streptavidin (SA, 1.8 µM), resulting in irreversible binding to antiSA even after the PBS

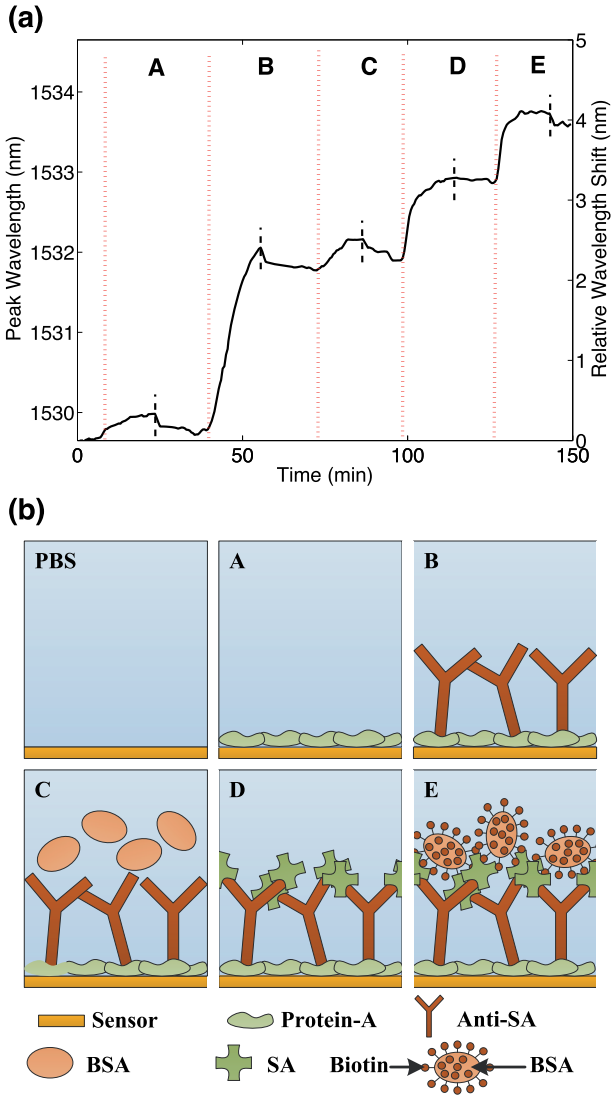

Figure 7 Biosensing experimental results: (**a**) depicts the resonance wavelength shifts as the experiment progressed while (**b**) illustrates reagent sequencing corresponding to regions [A–E] in (a). Region A = Protein-A (1 mg/mL), B = anti-streptavidin (SA) (125 μg/mL), C = Bovine Serum Albumen (BSA) (2 mg/mL), D = streptavidin (SA) (1.8 μM), E = Biotin-BSA (2.5 mg/mL). Introduction of reagent in each region was followed by a PBS-wash, as shown by the short, black-dashed line mid-way through each region.

rinse, as shown in region [D]. Finally, to illustrate a secondary amplification step, capture of biotinylated BSA (b-BSA, 2.5 mg/mL) to the immobilized SA is shown in region [E]. To validate that the wavelength shifts are as expected, we performed a quantitative analysis on the first protein monolayer based on observations by Coen et al. [43]. They determined coverage of the first monolayer on the waveguide surface to be 10–50% and that the successful immobilization of an IgG's Fc domain to a Protein-A receptor occurred on the second or third add layer. This presents a challenge in quantifying an exact number of bound molecules, especially for subsequent steps where molecules have multiple binding domains that may or may not be occupied. In addition, Claes et. al. discovered that biomolecules do not completely adhere and bind within the slot [19], creating additional uncertainty for an accurate analysis. Using Lumerical MODE solver, we modelled a 1 nm thick monolayer of Protein-A (42 kDa with a RI = 1.48 [44]) assuming: (1) moderate packing density on the waveguide surface due to steric hindrances, (2) limited diffusion into the slot, and (3) a sparse 3 nm film representing the second add layer. The simulated wavelength shift is twice the experimentally observed value, indicating 50% surface coverage with a 1 nm film. Based on the relative size and molecular weights of the subsequent molecules [45, 46], the resulting proportional wavelength shifts are also as expected. This simple assay demonstrates the specific and selective biosensing capability of our novel sensor and its potential for use in clinically relevant diagnostic settings.

4. Conclusion

In summary, we have designed, fabricated and characterized a novel silicon photonic biosensor using phase-shifted Bragg gratings in a slot waveguide. By easily integrating the waveguide sensor with microfluidic channels, we experimentally obtained a high sensitivity of 340 nm/RIU and a high Q factor of 1.5×10^4, which together result in a low intrinsic LOD of 3×10^{-4} RIU. This sensor also has a compact size, a large extinction ratio, and a large range for RI change. Finally, the sensor is successfully fabricated using a CMOS-compatible process, showing great potential for high-volume and low-cost production. Future work will include the integration of this sensor in architectures that allow for multiplexing and reference sensors, ultimately enabling more sophisticated label-free assays. In addition, surface functionalization strategies and chemistries we recently published in [47] will be explored to demonstrate its capability as a medical diagnostic sensor for use in complex media like saliva, serum, and whole blood.

Acknowledgements The authors would like to thank CMC Microsystems for enabling the fabrication of the silicon chips via ePIXfab, Lumerical Solutions, Inc. for providing the simulation software, Tom Baehr-Jones and Michael Hochberg (previously at the University of Washington and now at the University of Delaware) for kindly providing their experimental setup, and the Centre for High-Throughput Phenogeomics at the University of

British Columbia (UBC) for the assistance with the SEM images. We are also grateful to Prof. Nicolas A. F. Jaeger at UBC for his insights and support. This work was supported by the Natural Sciences and Engineering Research Council of Canada, the University of Washington (UW) Royalty Research Fund, NSF CBET (Award No. 0930411), and the Washington Research Foundation.

Author biographies Please see Supporting Information online.

References

[1] L. Chrostowski, S. Grist, J. Flueckiger, W. Shi, X. Wang, E. Ouellet, H. Yun, M. Webb, B. Nie, Z. Liang, K. C. Cheung, S. A. Schmidt, D. M. Ratner, and N. A. F. Jaeger, Proc. SPIE **8236**, 823620 (2012).
[2] H. K. Hunt and A. M. Armani, Nanoscale **2**, 1544–1559 (2010).
[3] X. Fan, I. M. White, S. I. Shopova, H. Zhu, J. D. Suter, and Y. Sun, Anal Chim Acta **620**, 8–26 (2008).
[4] M. S. Luchansky and R. C. Bailey, Anal. Chem. **84**, 793–821 (2012).
[5] K. D. Vos, I. Bartolozzi, E. Schacht, P. Bienstman, and R. Baets, Opt. Express, **15**, 7610–7615 (2007).
[6] A. L. Washburn, L. C. Gunn, and R. C. Bailey, Anal. Chem. **81**, 9499–9506 (2009).
[7] M. Iqbal, M. A. Gleeson, B. Spaugh, F. Tybor, W. G. Gunn, M. Hochberg, T. Baehr-Jones, R. C. Bailey, and L. Cary Gunn, IEEE J. Sel. Top. Quantum Electron. **16**, 654–661 (2010).
[8] M. S. Luchansky and R. C. Bailey, Anal. Chem. **82**, 1975–1981 (2010).
[9] J. Flueckiger, S. Grist, G. Bisra, L. Chrostowski, and K. Cheung, Proc. SPIE **7929**, 79290I (2011).
[10] J. T. Kirk, G. E. Fridley, J. W. Chamberlain, E. D. Christensen, M. Hochberg, and D. M. Ratner, Lab Chip **11**, 1372–1377 (2011).
[11] M. S. McClellan, L. L. Domier, and R. C. Bailey, Biosensors and Bioelectronics **31**, 388–392 (2012).
[12] A. S. Jugessur, J. Dou, J. S. Aitchison, R. M. De La Rue, and M. Gnan, Microelectronic Engineering **86**, 1488–1490 (2009).
[13] M. Lee and P. M. Fauchet, Opt. Express **15**, 4530–4535 (2007).
[14] S. Mandal and D. Erickson, Opt. Express **16**, 1623–1631 (2008).
[15] D. Threm, Y. Nazirizadeh, and M. Gerken, J. Biophoton. **5**, 601–616 (2012).
[16] V. R. Almeida, Q. Xu, C. A. Barrios, and M. Lipson, Opt. Lett. **29**, 1209–1211 (2004).
[17] F. Dell'Olio and V. M. N. Passaro, Opt. Express **15**, 4977–4993 (2007).
[18] C. A. Barrios, K. B. Gylfason, B. Sanchez, A. Griol, H. Sohlstrom, M. Holgado, and R. Casquel, Opt. Lett. **32**, 3080–3082 (2007).
[19] T. Claes, J. Molera, K. De Vos, E. Schacht, R. Baets, and P. Bienstman, IEEE Photonics J. **1**, 197–204 (2009).
[20] I. M. White and X. Fan, Opt. Express **16**, 1020–1028 (2008).
[21] T. Baehr-Jones, M. Hochberg, C. Walker, and A. Scherer, Appl. Phys. Lett. **86**, 081101 (2005).
[22] B. Wang, M. A. Dundar, R. Notzel, F. Karouta, and S. He, Appl. Phys. Lett. **97**, 151105 (2010).
[23] M. Scullion, A. D. Falco, and T. Krauss, Biosens. Bioelectron. **27**, 101–105 (2011).
[24] P. Prabhathan, V. M. Murukeshan, Z. Jing, and P. V. Ramana, Opt. Express **17**, 15330–15341 (2009).
[25] H.-C. Kim, K. Ikeda, and Y. Fainman, J. Lightwave Technol. **25**, 1147–1151 (2007).
[26] X. Wang, W. Shi, S. Grist, H. Yun, N. A. F. Jaeger, and L. Chrostowski, in: IEEE Photon. Conf., Arlington, Virginia, USA, October 2011, pp. 869–870.
[27] P. Dumon, W. Bogaerts, R. Baets, J.-M. Fedeli, and L. Fulbert, Electron. Lett. **45**, 581–582 (2009).
[28] M. Hochberg and T. Baehr-Jones, Nature Photon. **4**, 492–494 (2010).
[29] A. Yariv and P. Yeh, Photonics: Optical Electronics in Modern Communication (Oxford University Press, New York, 2007), p. 559.
[30] http://www.epixfab.eu.
[31] X. Wang, W. Shi, R. Vafaei, N. A. F. Jaeger, and L. Chrostowski, IEEE Photon. Tech. Lett. **23**, 290–292 (2011).
[32] X. Wang, W. Shi, H. Yun, S. Grist, N. A. F. Jaeger, and L. Chrostowski, Opt. Express **20**, 15547–15558 (2012).
[33] W. Shi, X. Wang, W. Zhang, H. Yun, C. Lin, L. Chrostowski, and N. A. F. Jaeger, Appl. Phys. Lett. **100**, 121118 (2012).
[34] X. Wang, W. Shi, M. Hochberg, K. Adam, E. Schelew, J. F. Young, N. A. F. Jaeger, and L. Chrostowski, in IEEE Group IV Photon. Conf., San Diego, California, USA, August 2012, pp. 288–290.
[35] F. Van Laere, T. Claes, J. Schrauwen, S. Scheerlinck, W. Bogaerts, D. Taillaert, L. O'Faolain, D. V. Thourhout, and R. Baets, IEEE Photon. Tech. Lett. **19**, 1919–1921 (2007).
[36] J. Blasco and C. Barrios, in: Conference on Lasers and Electro-Optics Europe, Munich, Germany, June 2005, p. 607.
[37] Y. N. Xia and G. M. Whitesides, Annu. Rev. Mater. Sci., **28**, 153–184 (1998).
[38] C. A. Barrios, M. J. Bañuls, V. González-Pedro, K. B. Gylfason, B. Sánchez, A. Griol, A. Maquieira, H. Sohlström, M. Holgado, and R. Casquel, Opt. Lett. **33**, 708–710 (2008).
[39] K. B. Gylfason, C. F. Carlborg, A. Kaźmierczak, F. Dortu, H. Sohlström, L. Vivien, C. A. Barrios, W. van der Wijngaart, and G. Stemme, Opt. Express **18**, 3226–3237 (2010).
[40] C. F. Carlborg, K. B. Gylfason, A. Kaźmierczak, F. Dortu, M. J. Bañuls Polo, A. Maquieira Catala, G. M. Kresbach, H. Sohlström, T. Moh, L. Vivien, J. Popplewell, G. Ronan, C. A. Barrios, G. Stemme, and W. van der Wijngaart, Lab Chip **10**, 281–290 (2010).
[41] W. L. DeLano, A. M. de Vos, M. H. Ultsch, and J. A. Wells, Science, **287**, 1279–1283 (2000).

[42] G. Moţa, I. Moraru, J. Sjöquist, and V. Gheţie, Mol. Immunol. **18**, 373–378 (1981).
[43] M. C. Coen, R. Lehmann, P. Gröning, M. Bielmann, C. Galli, and L. Schlapbach, J. Colloid Interface Sci. **233**, 180–189 (2001).
[44] J. Vörös, Biophys. J. **87**, 553–561 (2004).
[45] S. A. Darst, M. Ahlers, P. H. Meller, E. W. Kubalek, R. Blankenburg, H. O. Ribi, H. Ringsdorf, and R. D. Kornberg, Biophys. J. **59**, 387–396 (1991).
[46] A. Weisenhorn, F. J. Schmitt, W. Knoll, and P. Hansma, Ultramicroscopy **42**, 1125–1132 (1992).
[47] J. T. Kirk, N. D. Brault, T. Baehr-Jones, M. Hochberg, S. Jiang, and D. M. Ratner, Biosensors and Bioelectronics, **42**, 100–105 (2012).

